AIAA 91-0613
Turbulence Modeling Near the Free Surface in an Open Channel Flow

T.F. Swean, Jr., R.I. Leighton†, R.A. Handler,
and J.D. Swearingen

Center for Advanced Space Sensing,
Naval Research Laboratory,
Washington, D.C.

†Science Applications International Corp.,
McLean, Va.

29th Aerospace Sciences Meeting
January 7-10, 1991/Reno, Nevada

TURBULENCE MODELING NEAR THE FREE SURFACE IN AN OPEN CHANNEL FLOW

T.F. Swean, Jr.,† R.I. Leighton,* R.A. Handler,+ J.D. Swearingen+
Center For Advanced Space Sensing
Naval Research Laboratory
Washington, D.C. 20375-5000

Abstract

The velocity data from a direct numerical simulation of low Reynolds number turbulence in an open channel have been used to compute the terms in the budget equations for the turbulence kinetic energy, the dissipation of turbulence kinetic energy and the Reynolds stresses. The budget data show that the dissipation rates of the horizontal components of the turbulence are reduced near the surface while the dissipation of the vertical component remains approximately constant. The data also show that the pressure-strain term is the dominant producing term for the spanwise component of energy in the near surface region. A model for this behavior valid for flows exhibiting homogeneity in the spanwise and streamwise directions is proposed and tested against the data. In general the model is found to work well but wider testing is necessary.

Nomenclature

a_{ij}	= Reynolds stress anisotropy
A_α, A, A'	= functions of a_{ij}
a_α, b_α, etc.	= terms in Eqs. (5)
C_α	= model constant
g	= gravitational constant
h	= channel height
k	= turbulence kinetic energy
ℓ^*	= ν/u_τ, viscous length scale
p	= fluctuating pressure
$p^{(\alpha)}$	= defined in Eqs (8a,b)
Re_h	= $\bar{U}_s h/\nu$, Reynolds number
R^*	= $u_\tau h/\nu$, wall Reynolds number
S_{ij}	= mean strain rate
t^*	= ν/u_τ^2, viscous timescale
$\mathbf{U}$	= instantaneous velocity vector
U_i	= instantaneous velocity component
u_i	= fluctuating velocity component
u_τ	= $\sqrt{\tau_w/\rho}$, friction velocity
u^+	= $\bar{U}_1/u_\tau$
x_i	= coordinate direction
x_2^+	= $x_2 u_\tau/\nu$
y	= $1 - x_2$
δ_{ij}	= Kronecker's delta
ϵ	= isotropic dissipation function
$(\bar{\theta})$	= averaged quantity
ν	= kinematic viscosity
$\Phi^\beta_{ij,\alpha}$	= decomposed pressure strain, Eq. (9)
ρ	= density
τ	= shear stress
$\mathbf{\Omega}$	= instantaneous vorticity vector
Ω_i	= instantaneous vorticity component
Π^β_α, etc.	= terms in Eqs. (6,7)

Subscripts

i	= 1, 2, 3, coordinate directions
s	= value at free surface
w	= value at wall

1. Introduction

The turbulent flow below a gas-liquid interface plays an important role in diverse areas ranging from environmental flows and industrial mixing processes to the remote sensing of ship wakes. The near-boundary influences upon transfer and diffusion at the interface are of primary concern in environmental and industrial applications, whereas remote sensing issues ultimately involve any surface motions that may be detectable. For example, the two most common and persistent features seen in synthetic-aperture-radar images of ship wakes are bright "narrow vees" and long dark "scars", which may be a result of surface Bragg wave generation or modification through interactions with near surface turbulence. Common to all of these problems is the need for a better understanding of the structure of turbulence below a free surface

For several decades it has been realized that the presence of a free surface influences the evolution of mean velocity and turbulence but the mechanisms have not been completely described. Early observations of Nikuradse[1] showed the flow in straight open channels to be three-dimensional and that the maximum of the streamwise mean velocity occurs below rather than coincident with the free surface. More recently, the studies of Ueda[2] and Komori et al.[3] for open channel flows showed that the eddy viscosity is significantly attenuated by the presence of the free

† Research Mechanical Engineer, NRL, Member AIAA
* Research Scientist, SAIC, McLean, VA. 22102
+ Mechanical Engineer, NRL

surface. In the latter paper it is also shown that in a region near the free surface the surface-normal velocity fluctuations are diminished while the fluctuations in the plane of the surface are increased. The largest increase in the near-surface region is in the spanwise component. This paper also indicates that the viscous dissipation, ϵ, has vanishingly small normal gradient near the free surface. A similar redistribution of the turbulence intensities was observed by Thomas and Hancock.[4] In their work a moving wall experiment was devised such that the wall moved at the velocity of the adjacent turbulent fluid so that no velocity gradients and shear stresses were present at the wall, conditions similar to those at an uncontaminated, waveless free surface. Damping of the velocity fluctuations in the wall-normal direction accompanied by an increase in the streamwise fluctuations was observed. The spanwise fluctuations were only slightly increased. In recent experimental studies by Ramberg et al.[5] and Swean et al.[6,7] single-point hot-film measurements of the velocity correlations were obtained near the free surface in a jet flow. These measurements also showed the existence of a thin layer near the free surface wherein the redistribution of turbulence energy occurred rapidly with most of the vertical component transferring into the spanwise component, an observation similar to that of Komori et al. referenced above.

All of the above experiments experienced problems in acquiring data very near the surface. The hot-film studies suffer from the effects of probe contamination and blockage brought about by the intrusive sensor near the boundary. Laser doppler velocimetry methods have problems due to reflection and refraction at the free surface. As a result of the experimental problems associated with obtaining reliable measurements near an air-water interface, the situation is that considerably less is known about the characteristics of turbulence near a free surface as opposed to flow near to solid walls.

Due to the interest and relevance of the problem, a direct numerical simulation of turbulent open channel flow has been performed by Leighton et al.[8] This paper is an analysis of time-averaged data from Leighton's calculation with the goal of evaluating and improving turbulence models for use in practical calculations of the near-surface flow. In the next section a brief description of the calculation is given.

2. Direct Numerical Simulation

The incompressible 3D Navier-Stokes equations were solved for initial and boundary conditions approximating a turbulent open-channel flow of water at $Re_h = 2340$ based on the channel depth, h, and the mean steady velocity at the free surface, $\bar{U}_s = \bar{U}_2(x_2 = h)$. The governing equations were recast in the manner suggested by Orzag and Patera[9] and implemented by Kim, Moin and Moser[10] for closed channel flow. The final equation system, in which the pressure has been eliminated, consists of a 4^{th} order equation for the vertical velocity,

$$\left(\frac{\partial \nabla^2}{\partial t} - \frac{\nabla^4}{Re_h}\right) U_2 = \left(\frac{\partial^2}{\partial x_1^2} + \frac{\partial^2}{\partial x_3^2}\right)(\mathbf{U} \times \mathbf{\Omega})_2 - \frac{\partial}{\partial x_2}\left(\frac{\partial}{\partial x_1}(\mathbf{U} \times \mathbf{\Omega})_3 + \frac{\partial}{\partial x_3}(\mathbf{U} \times \mathbf{\Omega})_1\right), \quad (1)$$

and a 2^{nd} order equation for the vertical vorticity,

$$\left(\frac{\partial}{\partial t} - \frac{\nabla^2}{Re_h}\right) \Omega_2 = \frac{\partial}{\partial x_3}(\mathbf{U} \times \mathbf{\Omega})_1 - \frac{\partial}{\partial x_1}(\mathbf{U} \times \mathbf{\Omega})_3, \quad (2)$$

where all variables are non-dimensionalized by h and $\bar{U}_s$ and bold-face type indicates vector quantities with $\mathbf{\Omega} = (\nabla \times \mathbf{U})$. Following solution of Eqs. (1,2), the streamwise and spanwise velocity components (U_1, U_3) are recovered from the incompressibility condition and the definition of vorticity.

The equations are solved after they are Fourier transformed in the streamwise (x_1) and spanwise (x_3) directions and Chebyshev transformed in the vertical direction (x_2). The calculations were performed on a $48 \times 65 \times 64$ grid in x_1, x_2, x_3 respectively, which allows the resolution of all essential turbulent scales without resort to subgrid models. With the geometry scaled by the channel height, the vertical, streamwise and transverse dimensions of the channel are 1, 4π and $3\pi/2$, respectively. In wall units the domain is $134\ell^* \times 1684\ell^* \times 632\ell^*$, where $\ell^* = h/R^*$ with $R^* = 134$. For comparison purposes a companion calculation was performed for a closed channel flow. For reasons of economy this calculation was at half the wall-normal resolution of the open channel case and was at a lower Reynolds number, $R^* = 125$. Nevertheless the qualitative behavior of the data for all aspects examined was identical to that reported by Mansour, Moin and Kim (henceforth MKM).[11] As such these closed channel data can serve in certain instances to compare qualitatively the different behavior in the open and closed channel simulations.

The boundary conditions are periodic on all dependent variables in the streamwise and spanwise directions. No slip conditions are used at the channel bottom while the free surface is approximated as a rigid free slip surface with vanishing shear. The shear-free rigid lid condition is an approximation to the exact free surface condition which is valid at low Froude number $(\bar{U}_s(gh)^{-.5})$ for a surface free of any contaminants. Leighton et al.[8] have estimated the surface displacement *a posteriori* from the results of

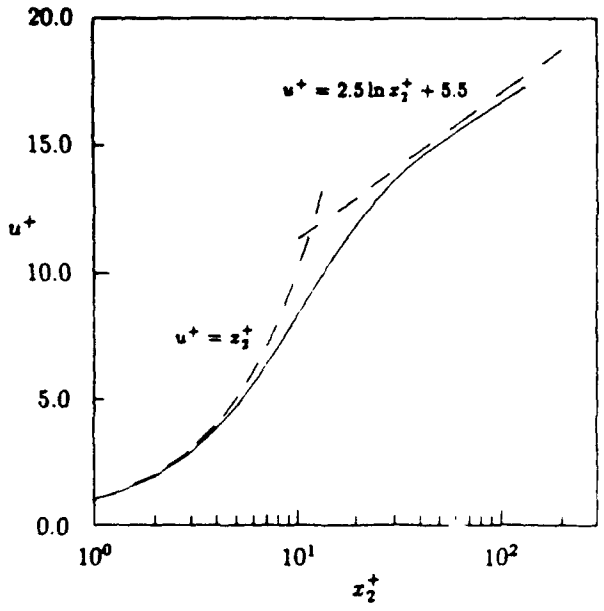

Fig. 1 Mean velocity profile across the channel.

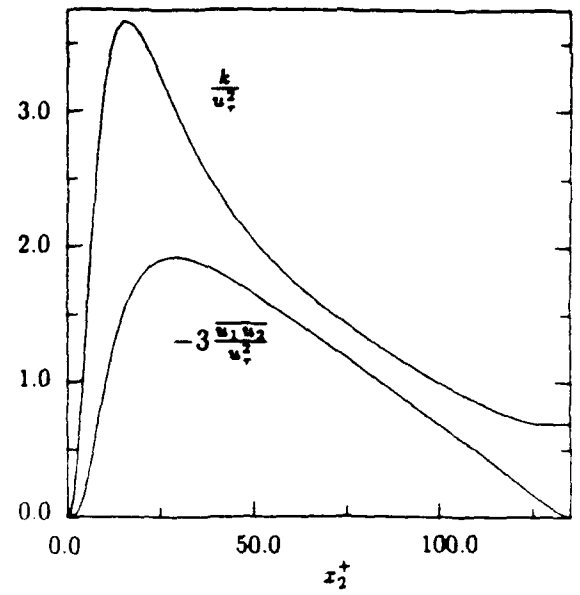

Fig. 2 Profiles of turbulence kinetic energy and Reynolds stress across the channel.

the simulation and using the channel height, $h = 0.04m$, from the experiments of Komori et al.[3] For these conditions the rms surface deflections could be expected to be approximately $1.6 \times 10^{-4}m$ $(0.004h)$ and negligible as observed in the laboratory experiments. For later reference the boundary values of the dependent and derived variables at the wall $(x_2 = 0)$ and free surface $(x_2 = 1)$ are:

$$U_1 = U_2 = U_3 = \Omega_2 = \frac{\partial U_2}{\partial x_2} = 0; x_2 = 0, \quad (3)$$

and

$$\frac{\partial U_1}{\partial x_2} = \frac{\partial U_3}{\partial x_2} = U_2 = \frac{\partial \Omega_2}{\partial x_2} = \frac{\partial^2 U_2}{\partial x_2^2} = 0; x_2 = 1. \quad (4)$$

The derivative conditions on U_2 arise from continuity considerations at the respective boundaries.

The computer code used in the simulation was designed and developed to run on the CRAY X-MP/24 at the Naval Research Laboratory. Approximately 10^{-5} seconds per timestep per grid point were required for the simulation. After the wall shear stress achieved a statistically steady behavior, 42 realizations of the instantaneous velocity data were saved during a time interval of approximately $4000t^*$ where $t^* = \nu/u_\tau^2$. Statistics were obtained by averaging in the streamwise and spanwise directions and in time.

3. Discussion of Results

The mean velocity normalized by u_τ is shown in Fig. 1. Also shown by the dashed lines are the wall laws $u^+ = x_2^+$ and $u^+ = 2.5 \ln x_2^+ + 5.5$. A best fit of the present data for the logrithmic region is $u^+ = 2.4 \ln x_2^+ + 5.6$. The lower slope is consistent with the value of 2.43 found by Nezu and Rodi[12] for open channel flows over a Reynolds number range $439 \leq R^* \leq 6139$. The intercept is near the upper bound (5.29 ± 0.47) found in their experiments and is probably a low Reynolds number effect.[11] The notable difference between the velocity data in Fig. 1 and closed channel behavior is the absence of a clearly defined wake region in the outer flow, rather the log law is maintained until very close to the free surface when the velocity adjusts to the vanishing gradient condition.

Figure 2 shows the normalized turbulence kinetic energy $k = \frac{1}{2}(\overline{u_1^2} + \overline{u_2^2} + \overline{u_3^2})$ and the Reynolds shear stress, $\overline{u_1 u_2}$, which has been further scaled for plotting by a factor as shown. According to the boundary conditions given by Eqs. (3,4) the velocity components and pressure can be expanded about the free surface as,

$$\begin{aligned} u_1 &= a_1 + c_1 y^2 + O(y^3) \\ u_2 &= b_2 y + d_2 y^3 + O(y^4) \\ u_3 &= a_3 + c_3 y^2 + O(y^3) \\ p &= a_p + c_p y^2 + O(y^3) \end{aligned} \quad (5)$$

where y is defined with the origin at the free surface. Use of these expansions and averaging results in $k = \frac{1}{2}(\overline{a_1^2} + \overline{a_3^2}) + O(y^2)$ near the surface and $\partial k/\partial y = 0$ at the surface which is evident in the figure.

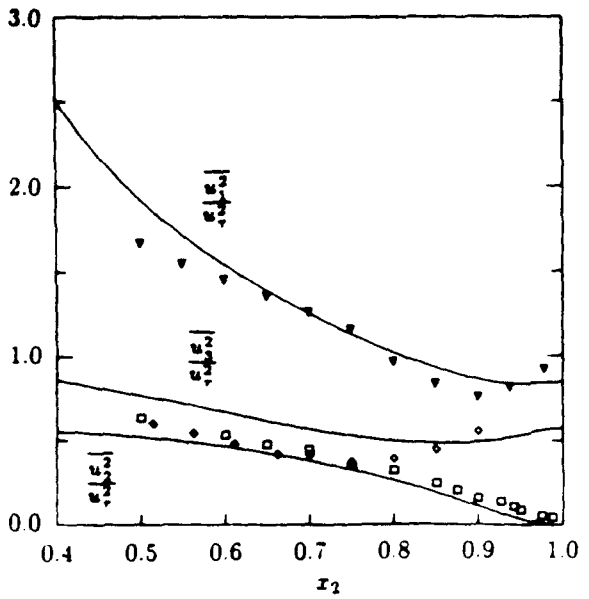

Fig. 3 Profiles of normal stresses across the channel and comparison with data of Komori et al.[3]

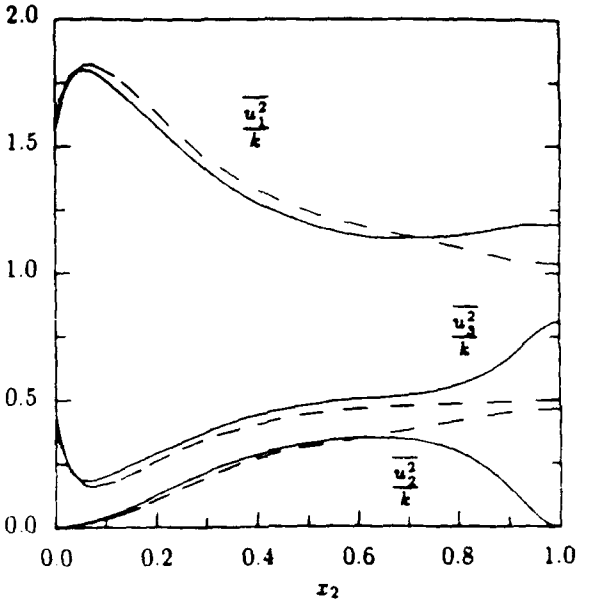

Fig. 4 Profiles of normal stresses normalized by the local value of turbulence kinetic energy. Dashed lines are from a closed channel simulation.

Figure 3 shows the three components of k from the simulation. The symbols are the experimental results of Komori et al.[3] which were taken at $Re_h \approx 3100$. There is qualitative agreement between the experimental and numerical results. Both exhibit an increase in the horizontal components as the free surface is approached and the increase is greatest for the spanwise component. The computed local minimum of the spanwise component occurs further from the free surface than in the streamwise component which is also consistent with the experiments. This behavior is more easily recognizable in Fig. 4 which contains the distributions of the three components of the turbulence kinetic energy made non-dimensional by the local value of k. Also shown in this figure are the data from the closed channel calculation referenced in the previous section and, as noted, these data are presented for qualitative comparison only. For the closed channel calculation the $x_2 = 1$ boundary corresponds to the channel centerline. Figure 4 shows that near the free surface, $x_2 > 0.7$, most of the energy from the vertical component is transferred to the spanwise component with only a small increase in the horizontal component. This contrasts with the behaviors of the various components of turbulence energy in the closed channel simulation where the relative interchange of energy appears to be primarily from the streamwise component to the vertical in the region near the channel centerline. In order to understand this behavior, the budget equations of the individual velocity correlations have been examined.

For the flow under consideration, which is statistically steady and homogeneous in the spanwise and streamwise directions, the transport equations for the one-point velocity correlations are,

$$\frac{D\overline{u_i u_j}}{Dt} = 0 = P_{ij} + \Pi_{ij} + T_{ij} + \Phi_{ij} + D_{ij} - \epsilon_{ij}. \quad (6)$$

The symbols on the right-hand side of Eq. (6) denote the rates of production, pressure diffusion, turbulent transport, pressure strain, viscous diffusion and dissipation, respectively. The explicit representations of these terms are:

$$P_{ij} = -\overline{u_i u_k}\frac{\partial \bar{U}_j}{\partial x_k} - \overline{u_j u_k}\frac{\partial \bar{U}_i}{\partial x_k},$$

$$\Pi_{ij} = -\frac{1}{\rho}\left(\frac{\partial \overline{pu_j}}{\partial x_i} + \frac{\partial \overline{pu_i}}{\partial x_j}\right),$$

$$T_{ij} = -\frac{\partial}{\partial x_k}\overline{u_i u_j u_k},$$

$$\Phi_{ij} = \overline{\frac{1}{\rho}p\left(\frac{\partial u_j}{\partial x_i} + \frac{\partial u_i}{\partial x_j}\right)},$$

$$D_{ij} = \nu\frac{\partial^2 \overline{u_i u_j}}{\partial x_k \partial x_k},$$

$$\epsilon_{ij} = 2\nu\overline{\frac{\partial u_i}{\partial x_k}\frac{\partial u_j}{\partial x_k}}.$$

The equation obtained by taking half the trace of Eq. (6) is the equation for the turbulence kinetic energy, k. The equation for the trace of the dissipation rate tensor, $\epsilon = (\epsilon_{11}+\epsilon_{22}+\epsilon_{33})/2$, is given by Hanjalic and Launder[13] as,

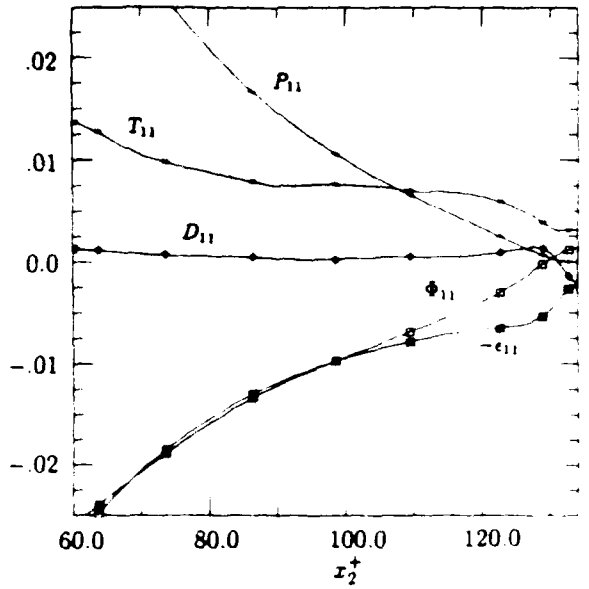

Fig. 5 Distribution of the terms in the budget of $\overline{u_1^2}$ in the upper half of the channel.

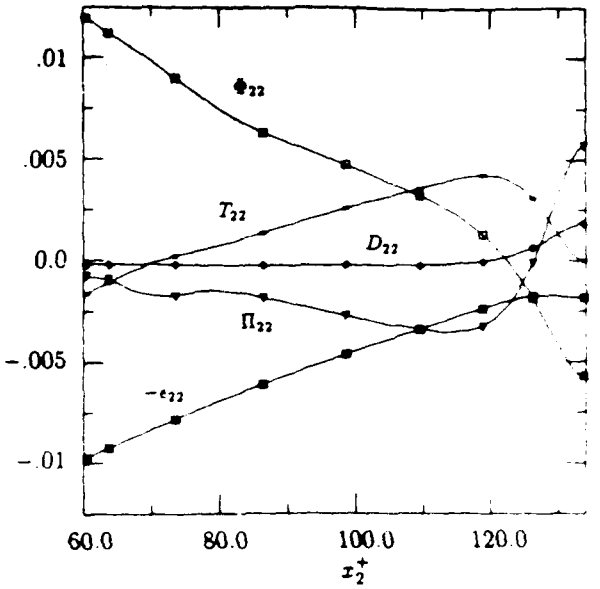

Fig. 6 Distribution of the terms in the budget of $\overline{u_2^2}$ in the upper half of the channel.

$$\frac{D\epsilon}{Dt} = 0 = -2\nu\left(\overline{\frac{\partial u_i}{\partial x_\ell}\frac{\partial u_k}{\partial x_\ell}}\right)\frac{\partial \bar{U}_i}{\partial x_k} - 2\nu\left(\overline{\frac{\partial u_\ell}{\partial x_i}\frac{\partial u_\ell}{\partial x_k}}\right)\frac{\partial \bar{U}_i}{\partial x_k}$$
$$-2\nu\overline{u_k\frac{\partial u_i}{\partial x_\ell}}\frac{\partial^2 \bar{U}_i}{\partial x_k \partial x_\ell} - 2\nu\overline{\frac{\partial u_i}{\partial x_k}\frac{\partial u_i}{\partial x_\ell}\frac{\partial u_k}{\partial x_\ell}}$$
$$-\frac{2\nu}{\rho}\frac{\partial}{\partial x_k}\left(\overline{\frac{\partial p}{\partial x_\ell}\frac{\partial u_k}{\partial x_\ell}}\right) - \nu\overline{\frac{\partial}{\partial x_k}u_k\left(\frac{\partial u_i}{\partial x_j}\frac{\partial u_i}{\partial x_j}\right)}$$
$$+\nu\frac{\partial^2 \epsilon}{\partial x_k^2} - 2\overline{\left(\nu\frac{\partial^2 u_i}{\partial x_k \partial x_\ell}\right)^2} \qquad (7)$$

The first four terms are production terms (P_ϵ^1 to P_ϵ^4), while terms five through eight are pressure transport (Π_ϵ), turbulent transport (T_ϵ), viscous diffusion (D_ϵ) and dissipation (Y), respectively.

The terms in the budget equations for the three normal stresses and the dissipation rate are shown in Figs. 5-8. All terms in Eqs. (6,7) have been normalized by u_τ^4/ν and the budgets are displayed only for the upper half of the channel nearest the free surface. Since the production of turbulence is much lower than in the high shear region close to the solid wall, the individual terms in the equations are typically an order of magnitude lower than their corresponding values near the wall. The near-wall data are available in Leighton et al.[8] and are very similar to the data of MKM.[11]

Figure 5 shows that away from the surface all terms in the $\overline{u_1^2}$ budget have the same relative importance except D_{11}, the viscous diffusion. Moving toward the surface, the production rate vanishes with the mean velocity gradient. At the wall, the viscous terms balance the turbulence transport and the pressure strain, the latter having become a slight positive contributor to the budget very near the wall. The $\overline{u_2^2}$ balance in Fig. 6 is relatively more complex than that for $\overline{u_1^2}$. For this component the magnitude of the budget terms near the free surface are only reduced by about one-half from their values near the solid wall. Near the free surface, the asymtotic behavior of the various terms can be determined by using Eqs. (5) as

$$T_{22} = -3\overline{b_2^3}y^2 + \cdots$$
$$\Pi_{22} = -2\overline{a_p b_2} - 6(\overline{c_p b_2} + \overline{a_p d_2})y^2 + \cdots$$
$$\Phi_{22} = 2\overline{a_p b_2} + 2(\overline{c_p b_2} + 3\overline{a_p d_2})y^2 + \cdots$$
$$D_{22} = 2\overline{b_2 b_2} + 24\overline{b_2 d_2}y^2 + \cdots$$
$$\epsilon_{22} = 2\overline{b_2 b_2} + 12\overline{b_2 d_2}y^2 + \cdots$$

It is seen that at the free surface ϵ_{22} balances D_{22} and the two pressure-velocity terms cancel. Note that the pressure strain has rapidly become a consuming term in the near-surface region whereas it had been a major producer in the budget equation in the outer flow. This is in contrast to the behavior shown in Fig. 7 for the $\overline{u_3^2}$ component. In this case Φ_{33} increases near the surface and at the surface is considerably more of a source for $\overline{u_3^2}$ than is Φ_{11} in the $\overline{u_1^2}$ budget. This largely explains why the transverse component of turbulence kinetic in Fig. 4 is increased relatively more so than the streamwise component as $\overline{u_2^2}$ approaches zero at the free surface. In the next section a model for this behavior is proposed.

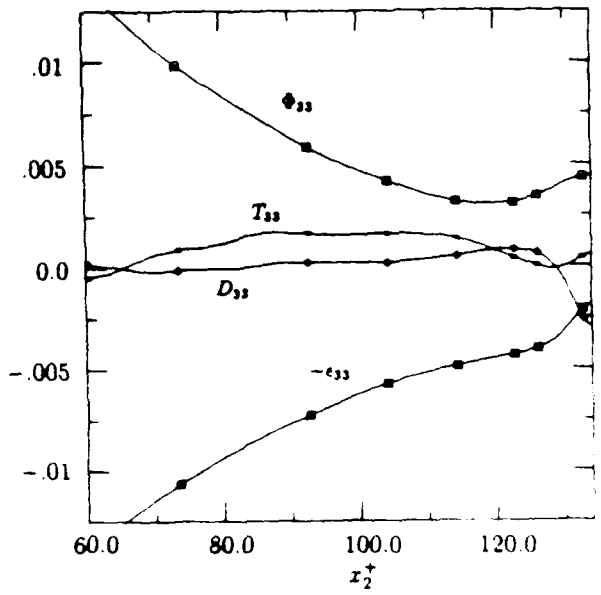

Fig. 7 Distribution of the terms in the budget of $\overline{u_3^2}$ in the upper half of the channel.

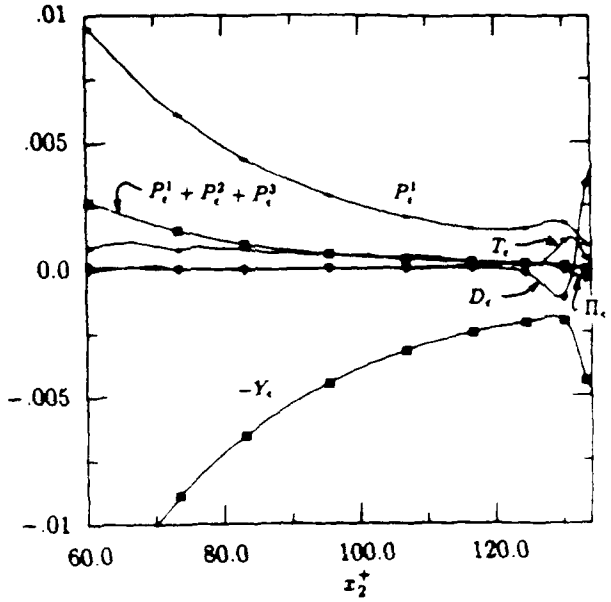

Fig. 8 Distribution of the terms in the budget of the turbulence kinetic energy dissipation rate in the upper half of the channel.

A curious feature contained in Figs. 5 and 7 is the behavior of ϵ_{ii} as the surface is approached. Moving toward the free surface the dissipation rates exhibit a sharp drop in magnitude in the upper 5-10% of the channel. The ϵ_{22} on the other hand shows a very slight increase in magnitude and could well be approximated as constant in this region. This behavior is contrary to standard modeling assumptions near the free surface. Hossain and Rodi[14] and later Naot and Rodi[15] have assumed that in most respects other than the vanishing of the surface-normal velocity component, the free surface behaves like a symmetry plane. The exception is the presumed behavior of the dissipation rate for turbulence kinetic energy which is expected to increase near the surface. This is based on the assumption that the macro-length scale of the turbulence ($L \propto k^{1.5}/\epsilon$) is reduced by the presence of the boundary. This scale does not become zero since it reflects the fluctuating motion in all three directions and the horizontal extent of the eddies is not restricted.

The terms in the budget equation for the dissipation rate are shown in Figure 8. In the upper portion of the channel the first three production terms in Eq. (7) are small and have been lumped together as shown. Until very near the free surface the production by turbulence, P_ϵ^4, largely balances the dissipation term. Very near the surface the dominant terms are the viscous diffusion and the dissipation, each exhibiting very large gradients of opposite sign near the boundary. Reconsidering Figs. 5 and 7, it is seen that in these cases also the rapid variation in the dissipation term appears to be at least partially offset by the variation in the diffusion term. It should be remembered that ϵ_{ii} (or ϵ) is not the actual dissipation of turbulent energy for inhomogeneous flows although it does approximate the total dissipation for high Reynolds number. The particular terms D_{ii} and ϵ_{ii} have arisen from the combination of the actual dissipation rate with the rate of work by the viscous shear stresses of the turbulence.[16] In flows far from solid walls the viscous diffusion is generally neglected and as such the modeled dissipation rate implicitly models the work term. Figure 9 shows the balance of turbulence kinetic energy obtained from the trace of Eq. (6). The viscous terms have been added and together they balance the transport terms at the wall. It is seen that the total viscous term varies only slightly near the boundary and might be easier to model. Future work will re-process the velocity data to determine the actual dissipation term separately from the work term.

4. Pressure-Strain Rate Model

The above data show that the pressure-strain term is a key contributor to the redistribution of normal stresses near the boundaries. Leighton et al.[8] have decomposed the fluctuating pressure into a 'slow' pressure, $p^{(1)}$, a 'fast' pressure, $p^{(2)}$, and a Stokes pressure, $p^{(s)}$, in the manner suggested by MKM.[11] These components satisfy the equations:

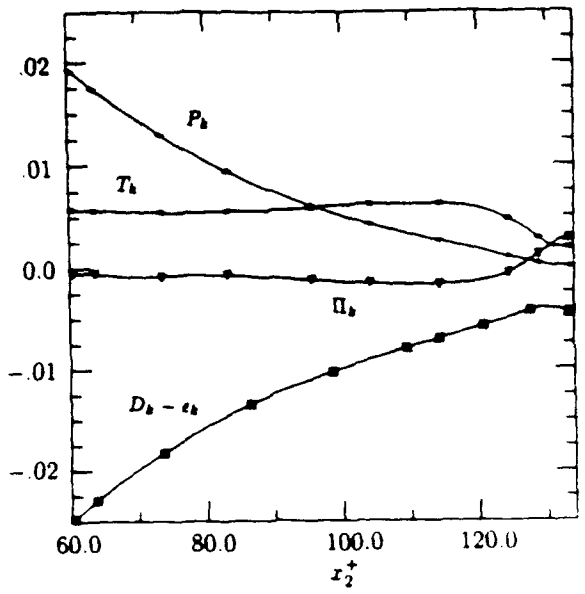

Fig. 9 Distribution of the terms in the budget of turbulence kinetic energy in the upper half of the channel.

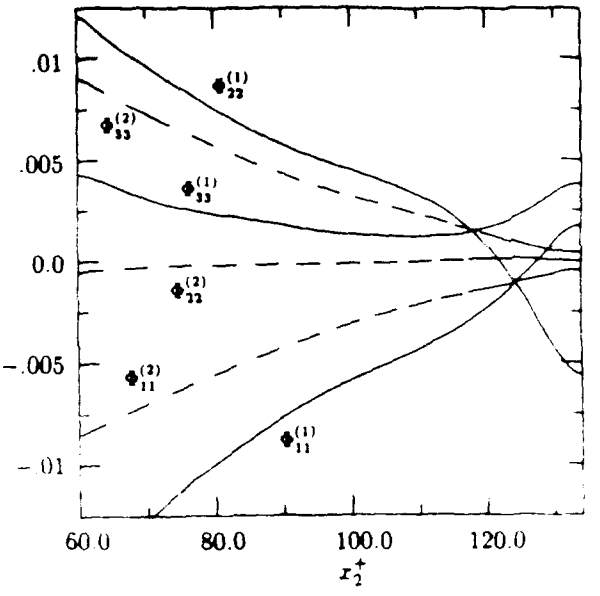

Fig 10 Distribution of the rapid and return contributions to the pressure-strain rate for each diagonal component.

$$\nabla^2 p^{(1)} = -\left(\frac{\partial u_i}{\partial x_j}\frac{\partial u_j}{\partial x_i} - \overline{\frac{\partial u_i}{\partial x_j}\frac{\partial u_j}{\partial x_i}}\right),$$
$$\nabla^2 p^{(2)} = -2\frac{\partial \bar{U}_1}{\partial x_2}\frac{\partial u_2}{\partial x_1}, \qquad (8a)$$
$$\nabla^2 p^{(s)} = 0,$$

with boundary conditions,

$$\frac{\partial p^{(1)}}{\partial x_2} = 0 \;:\; x_2 = 0, 1$$

$$\frac{\partial p^{(2)}}{\partial x_2} = 0 \;:\; x_2 = 0, 1 \qquad (8b)$$

$$\frac{\partial p^{(s)}}{\partial x_2} = \frac{1}{Re_h}\frac{\partial^2 u_2}{\partial x_2^2} \;:\; x_2 = 0, 1.$$

The pressure data from the solution of Eqs. (8a-b) have been used to decompose the pressure-strain term into

$$\Phi_{ii} = 2\overline{p\frac{\partial u_i}{\partial x_i}} = \Phi_{ii}^{(1)} + \Phi_{ii}^{(2)} + \Phi_{ii}^{(s)}$$

Figure 10 shows this splitting in the upper portion of the channel for each of the components. The Stokes term is only of consequence very near the solid wall and is not plotted. It is seen that the slow or return terms are dominant in the region plotted. Only in the Φ_{33} component is the fast term the larger of the two and for the Φ_{22} term the fast component is nearly zero over the whole domain shown.

The distributions of Φ_{ij} shown in Fig. 10 differ markedly at the free surface relative to their behavior at a solid wall.[11] Most importantly they do not vanish in any component. Clearly some sort of surface proximity effect is needed in order to model the rapid variations exhibited. Generally the total term is modeled,

$$\Phi_{ij} = \Phi_{ij}^{(1)} + \Phi_{ij}^{(2)} + \Phi_{ij,w}^{(1)} + \Phi_{ij,w}^{(2)} \qquad (9)$$

where $\Phi_{ij}^{(1)}$ is some variant of Rotta's[17] model.

$$\Phi_{ij}^{(1)} = -C_1\epsilon a_{ij}, \qquad (10)$$

and the rapid term includes at least the isotropization of production term, $(P_{ij} - \frac{2}{3}P_k\delta_{ij})$. Typical of these models and one that is borrowed from in the current study, is that due to Launder, Reece and Rodi[18]

$$\Phi_{ij}^{(2)} = -\frac{(C_2' + 8)}{11}(P_{ij} - \frac{2}{3}P_k\delta_{ij})$$
$$-2\frac{(30C_2' - 2)}{55}kS_{ij} - \frac{8(C_2' + 8)}{11}(B_{ij} - \frac{2}{3}P_k\delta_{ij}), \qquad (11)$$

where,

$$B_{ij} = -\overline{u_i u_k}\frac{\partial \bar{U}_k}{\partial x_j} - \overline{u_j u_k}\frac{\partial \bar{U}_k}{\partial x_i},$$

and $C_2' = 0.4$. The wall terms are usually modeled in a form analagous to Eqs. (10,11) but with different coefficients and including a damping function. The Launder, Reece and Rodi form is,

$$\Phi_{ij,w}^{(1)} + \Phi_{ij,w}^{(2)} = (0.125\epsilon a_{ij} + 0.015(P_{ij} - B_{ij}))\frac{k^{\frac{3}{2}}}{\epsilon x_2}$$

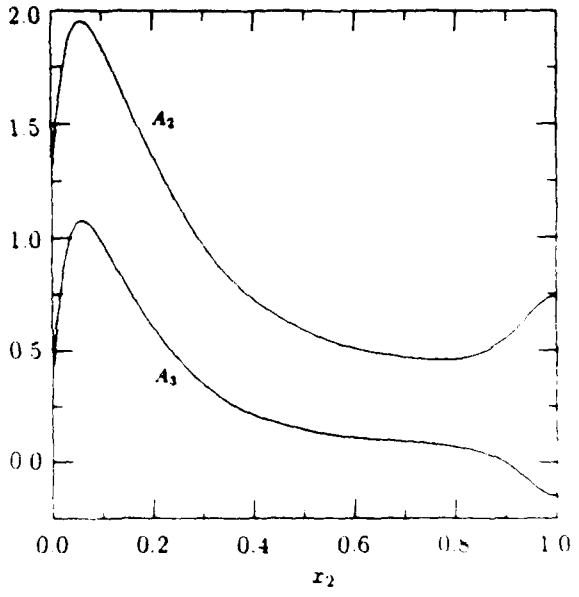

Fig. 11 Distribution of the second and third invariants of the Reynolds stress anisotropy tensor across the channel.

This particular damping function is singular at a free surface since k does not vanish. A virtual origin could be used and has been employed by Naot and Rodi[15]. An alternative is to use a term based on the surface-normal velocity such as $f_w \sim (\overline{u_2^2})^5 k/\epsilon x_2$, which does not become singular and is more appealing on physical grounds. However, the approach taken in this study is to make use of the properties of the second and third invariants, A_2 and A_3 of the stress anisotropy tensor, a_{ij},

$$A_2 \equiv a_{ij}a_{ij} \; ; \; A_3 \equiv a_{ij}a_{jk}a_{ki} \qquad (12)$$

As pointed out by Lumley[19], if one component of velocity vanishes, then the difference, $A_2 - A_3$, becomes the constant value 8/9 irrespective of the behavior of the other two velocity components. In this case the function $A \equiv 1 - 9(A_2 - A_3)/8 = 0$ in the regions where the turbulence becomes locally two-dimensional. At the free surface the pressure-strain rates do not vanish so it is necessary to modify this approach. Figure 11 shows the variation of A_2 and A_3 computed from the simulation data. Near both boundaries $A_2 - A_3 \rightarrow 8/9$ as $a_{22} \rightarrow -2/3$. Near the free surface it is observed that A_3 becomes negative. This is very close to the x_2 location where a_{33} becomes positive (see Fig. 4). For flows in which the non-zero velocity components remain uncorrelated as the third component vanishes, the vanishing of A_3 corresponds exactly to the vanishing of one of the remaining remaining a_{ii}. Equation (12) shows that for such a flow A_3 reaches a minimum of $-2/9$ when $a_{11} = a_{33}$. It is plausible to assume that in the absence of boundaries the horizontal components will tend to approach this state at a free surface. The available experimental data as well as the current simulation data support this conjecture. If this is the case then the vanishing of A_3 can be used as a detector for free surface proximity effects.

A model based on Lumley's suggestion and used as the basis of the current model is that due to Launder and Shima.[20] In their model $\Phi_{ij}^{(1)}$ is given by Eq. (10) with the coefficient,

$$C_1 = 2.58AA_2^{.25}\{1 - \exp((0.0067k^2/\nu\epsilon)^2)\} \qquad (13)$$

The rapid term is given by the first term in Eq. (11) with the coefficient, $8(C_2'+8)/11$, replaced with $C_2 = 0.75A^5$. The Launder and Shima model also contains additional explicit expressions for the wall terms in Eq. (9) that are not repeated here since they are not used.

In the current work an effort has been made to construct a model with a minimum of parameters. In Eq. (13), both the coefficient, A, and the term in braces containing the Reynolds number act to damp the pressure-strain rate near a solid wall. Equations (8a,b) are only dependent upon viscosity thru the boundary condition on the equation for p^* and MKM have shown that for low Reynolds flows of the type under study here, $\Phi_{ii}^{(*)}$ is small even near the wall. The term in braces has thus been omitted in the current study. Exploratory calculations retaining the term, and using the statistics from the simulation, have shown that the term has little effect on model performance and in fact the pressure-strain rate data are better correlated with its omission. Although the concern here has not been model performance near the solid wall, this study has also retained the third term in Eq. (11) since its inclusion substantially improves the behavior in the Φ_{22} component near the wall. The basic form of the current model then becomes,

$$\Phi_{ij}^{(1)} = -C_1 A\epsilon a_{ij} \; ; \; C_1 \equiv 1.3A_2^{.25}. \qquad (14)$$

$$\Phi_{ij}^{(2)} = A_2^{.5}\Big(-\frac{(C_2'+8)}{11}\Big(P_{ij} - \frac{2}{3}P_k\delta_{ij}\Big) - \frac{8(C_2'+8)}{11}\Big(B_{ij} - \frac{2}{3}P_k\delta_{ij}\Big)\Big) \qquad (15)$$

The numerical value in the definition of C_1 above has been adjusted from its former value to account for the factor of approximately 1/2 that the retention of the exponential term of the original model would have contributed in the outer flow. The form adopted for the free surface region is,

$$\Phi_{ij,s}^{(1)} = -C_1(A - A')\epsilon(2.2a_{ij} + 9.8(a_{ik}a_{kj} - A_2/3)) \qquad (16)$$

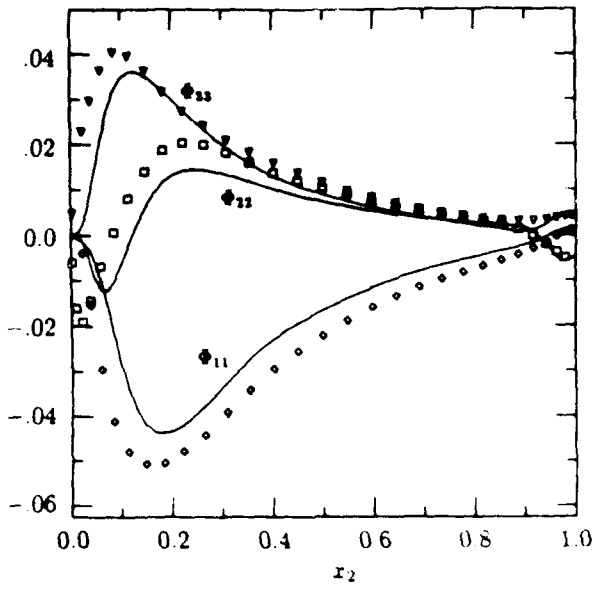

Fig. 12 Comparison of the modeled pressure-strain rate with the data from the simulation

where C_1 is given by Eq. (14) and $A' \equiv 1 - 9/8(A_2 - |A_3|)$. As discussed earlier this term will only become active when the anisotropy in one of the horizontal components vanishes while the vertical velocity is damped near the free surface. The constants 2.2 and 9.8 have been determined so as match the overall level of the data in the surface region. The 2^{nd} order term has been shown by Speziale et al.[21] to occur in a formal expansion for Φ_{ij} and it is used in the current formulation to achieve more closely the separation in Φ_{33} and Φ_{11} observed in the simulation. Near the free surface the anisotropy in the u_3 component of velocity is relatively small compared to a_{11} so to first order in anisotropy the model predicts that $\Phi_{11} > \Phi_{33}$. The second order term is small in both components but has a much greater relative effect on the u_3 component.

Figure 12 shows the model performance when computed with the simulation data which are represented by the symbols. The lines are computations with Eqs. (14-16). The incorrect near-surface asymtotic behavior is mostly due to the sharp variation in ϵ discussed in the previous section. Incorporating the proper asymtotic behavior near the free surface will be a topic for further research. Near the solid wall the current model performs reasonably well and markedly better than the original Launder, Reece and Rodi model which was analyzed by MKM.[11] The asymtotic behavior near the wall is not correct and this must be examined as well. Without the inclusion of the term containing B_{ij} in Eq. (15) the change in sign in the near wall region for Φ_{22} is not achieved but rather the modeled distribution is uniformly positive until vanishing at the wall.

5. Concluding Remarks

The simulation data show that there is a preferential redistribution of turbulence energy to the spanwise component of energy as the normal component is damped at the free surface. This is in accordance with the still-limited experimental observations. The budget equations show that the pressure-strain rate term, particularly the return term, is a key contributor to this behavior. The budgets also show that the isotropic part of the dissipation of turbulence enery decreases rapidly very near the free surface which is contrary to current modeling asumptions which assume it to increase to account for reduced levels of eddy viscosity observed near the free surface. A model for the near-surface pressure-strain term has been proposed and shown to correlate the simulation data fairly well. In its current form the model is limited to flows in which the correlation of the horizontal velocity components is small while the vertical component vanishes. Much wider testing is necessary to determine when this condition exists. Future efforts will consider this point along with questions raised regarding the dissipation of turbulence at the surface

Acknowledgements

This work is supported by the Naval Research Laboratory under the Core fluid mechanics program and the Office of Naval Research under the Surface Ship Wake Detection Program. Many of the calculations were performed under an NRL Cray Grant The authors acknowledge the many fruitful discussions with Dr. Jeff Crouch.

References

[1]Nikuradse, J., "Turbulente Strömung im Innern des rechteckigen offenen Kanals", Forschungsarbeiten, Heft 281, 1926, pp. 36-44.

[2]Ueda, H., "Eddy Diffusivity Near the Free Surface of Open Channel Flow", *International Journal of Heat and Mass Transfer*, Vol 20, No. 11, 1977 pp. 1127-1136.

[3]Komori, S., Ueda H., Ogino, F. and Mizushina, T., "Turbulence Structure and Transport Mechanism at the Free Surface in an Open Channel Flow", *International Journal of Heat and Mass Transfer*, Vol. 25, No. 4, 1982, pp. 513-521.

[4]Thomas, S.M. and Hancock, P.E., "Grid Turbulence Near a Moving Wall", *Journal of Fluid Mechanics*, Vol. 82, 1977, pp. 481-496.

[5]Ramberg, S.E., Swean, T.F., Jr. and Plesniak M.W., "Turbulence Near a Free Surface in a Plane Jet", NRL Memorandum Report No. 6367, 1989.

[6]Swean, T.F., Jr., Ramberg, S.E., Plesniak M.W. and Stewart, M.B., "Turbulent Surface Jet in

Channel of Limited Depth", *ASCE Journal of Hydraulic Engineering*, Vol. 115, No. 12, 1989, pp. 1587-1606.

[7]Swean, T.F., Jr., Ramberg, S.E. and Miner, E.W., "Anisotropy in a Turbulent Jet Near a Free Surface" *ASME Journal of Fluids Engineering*, to appear 1991.

[8]Leighton, R.I., Swean, T.F., Jr., Handler, R.A. and Swearingen, J.D. "Direct Simulation of Low Reynolds Number Open Channel Flow", NRL Memorandum Report, 1991.

[9]Orszag, S.A. and Patera, A.T., "Subcritical Transition to Turbulence in Planar Shear Flows" in *Transition and Turbulence*, ed. by R.E. Myer, Academic Press, London, New York, 1981, pp. 127-146.

[10]Kim, J., Moin, P. and Moser, R., "Turbulence Statistics in a Fully Developed Channel Flow at Low Reynolds Number", *Journal of Fluid Mechanics*, Vol. 177, 1987, pp. 133-136.

[11] Mansour, N.N., Moin, P. and Kim, J., "Reynolds-Stress and Dissipation-Rate Budgets in a Turbulent Channel Flow", *Journal of Fluid Mechanics*, Vol. 194, 1988, pp. 15-44.

[12]Nezu, I. and Rodi, W., "Open-Channel Flow Measurements With a Laser Doppler Anemometer", *ASCE Journal of Hydraulic Engineering*, Vol. 112, No. 5, 1986, pp.335-355.

[13]Hanjalić, K. and Launder, B.E., "Contribution Towards a Reynolds-Stress closure for Low-Reynolds-Number Turbulence", *Journal of Fluid Mechanics*, Vol. 74, 1976, pp.593-610.

[14]Hossain, M.S. and Rodi, W., " Mathematical Modelling of Vertical Mixing in Stratified Channel Flow" , *Proceedings, Second Symposium on Stratified Flows*, Trondheim, Norway, 1980.

[15]Naot, D. and Rodi, W., "Calculation of Secondary Currents in Channel Flow", *ASCE Journal of Hydraulic Engineering*, Vol. 108, No. HY8, 1982, pp. 948-968.

[16]Hinze, J.O., *Turbulence*, McGraw-Hill, New York, 1975.

[17]Rotta,J.C., "Statistical Theorie Nichomogener Turbulenz", *Zeitschrift fur Physik*, Vol 129, 1951, p.547.

[18]Launder, B.E., Reece, G.J. and Rodi, W.,"Progress in the Development of a Reynolds-Stress Turbulence Closure", *Journal of Fluid Mechanics*, Vol. 68, 1975, pp. 537-565.

[19]Lumley, J.L., "Computational Modeling of Turulen t Flows", *Advances in Applied Mechanics*, Vol. 18, 1978, p.123-176.

[20]Launder, B.E. and Shima, N., "Second-Moment Closure for the Near-Wall Sublayer: Development and Application", *AIAA Journal*, Vol. 27, No. 10, 1989, p.1319-1325.

[21]Speziale, C.G., Sutanu, S. and Gatski, T.B., "Modeling the Pressure-Strain Correlation of Turbulence – An Invariant Dynamical Systems Approach", NASA Contractor Report 181979, ICASE Report No. 90.5, 1990.